Coupled spherical-cavities

Cite as: AIP Advances 12, 125022 (2022); https://doi.org/10.1063/5.0084815 Submitted: 19 January 2022 • Accepted: 31 August 2022 • Published Online: 21 December 2022

Stanislav Kreps, D Vladimir Shuvayev, Mark Douvidzon, et al.

COLLECTIONS



This paper was selected as an Editor's Pick









AIP Advances

Energy Collection



Coupled spherical-cavities

Cite as: AIP Advances 12, 125022 (2022); doi: 10.1063/5.0084815 Submitted: 19 January 2022 • Accepted: 31 August 2022 • Published Online: 21 December 2022







Stanislav Kreps,^{1,a)} Vladimir Shuvayev,² Mark Douvidzon,¹ Baheej Bathish,¹ Tom Lenkiewicz Abudi,¹ Amirreza Ghaznavi,³ Jie Xu,³ Yang Lin,⁴ Lev Deych,⁵ Dand Tal Carmon⁶ D

AFFILIATIONS

- Department of Mechanical Engineering, Technion-Israel Institute of Technology, 3200003 Haifa, Israel
- ²Physics Department, Queens College of CUNY, Flushing, Queens, New York 11367, USA
- ³University of Illinois at Chicago, Chicago, Illinois 60607, USA
- ⁴University of Rhode Island, Kingston, Rhode Island 02881, USA
- ⁵The Graduate Center of CUNY, 365 5th Ave., New York, New York 10016, USA
- ⁶School of Electrical Engineering, Tel Aviv University, Tel Aviv, Israel

ABSTRACT

In this work, we study theoretically and experimentally optical modes of photonic molecules—clusters of optically coupled spherical resonators. Unlike previous studies, we do not use stems to hold spheres in their positions relying, instead, on optical tweezers to maintain desired structures. The modes of the coupled resonators are excited using a tapered fiber and are observed as resonances with a quality factor as high as 10⁷. Using the fluorescent mapping technique, we observe families of coupled modes with similar spatial and spectral shapes repeating every free spectral range (a spectral separation between adjacent resonances of individual spheres). Experimental results are compared with the results of numerical simulations based on a multi-sphere Mie theory. This work opens the door for developing large arrays of coupled high-Q spherical resonators.

© 2022 Author(s). All article content, except where otherwise noted, is licensed under a Creative Commons Attribution (CC BY) license (http://creativecommons.org/licenses/by/4.0/). https://doi.org/10.1063/5.0084815

I. INTRODUCTION

Microcavities¹⁻³ were used in various optical applications^{4,5} as well as in fundamental studies, which take advantage of the resonance enhancement of electromagnetic field density to study new regimes of interaction between light and matter, 6-8 structure vibrations, 9,10 sound, 11,12 and even water waves. 13 Coupled resonators 14-22 have also been used to study non-reciprocity, 23 broadband filters, 24,25 modulators, 26 and sensors. 27 Most previous studies of photonic molecules dealt mainly with two-resonator structures, where thermal tuning was used to achieve the spectral overlap required to achieve efficient optical coupling.²⁸ Coupling of more than two high-Q cavities²⁹ was rare because it was difficult to achieve spectral overlap between resonances belonging to different resonators.³⁰ It shall also be noted that most of the existing studies were limited to two-dimensional configurations such as disks,³¹ rings,²⁷ or toroids,²³ which could be fabricated by welldeveloped planar fabrication techniques³¹ and convenient for optical and electronic integration. However, the planar structures are

limited in the number and the character of modes, which they can sustain.

In this work, we fabricate and study three-dimensional structures of three or more spherical resonators exhibiting a rich variety of optical modes. The developed approach can also be extended to arrays of a larger number of spherical resonators arranged in any predefined configuration such as, e.g., a bodycentered cubic (BCC) crystal lattice or an amorphous structure with pre-designed correlation properties. Unlike previous studies that dealt with spherical resonators positioned using a mechanical clapping device like a stem³² or a pillar³³ to support them, we are using optical tweezers to maintain the desired configuration of the constituent resonators.³⁴ The reliance on optical tweezers allowed us to avoid significant limitations on the allowed regions where modes can exist imposed by mechanical clapping so that we can excite a greater number of modes with a variety of spatial configurations.

Modes of a single sphere are highly degenerate and can be thought of as originating from closed paths taken by a light ray

^{a)}Author to whom correspondence should be addressed: kr.stanislav@campus.technion.ac.il

traveling along the sphere's great circles with different modes corresponding to different orientations of the plane containing the ray trajectory. In multiple sphere systems, the spherical symmetry is destroyed together with the degeneracy of the modes. Thus, the modes of the photonic molecules are characterized by various relatively complex distributions of the electromagnetic field, which can be thought to originate from complex ray trajectories traversing all participating spheres. When a coupled multi-sphere system is excited using a tapered fiber, such as in Fig. 1, the excitation of the resonances manifests itself by destructive interference of the incident light with light propagating out of the resonators and are observed as minima in the optical transmission.

We study the modes of the coupled resonators both in frequency and spatial domains. In the spatial domain, we experimentally map the resonances using a fluorescent mode-mapping technique. 35-37 In the frequency domain, we experimentally measure the transmission spectrum of the sphere array using a tunable laser source. The photographs of the fluorescent emission, as well as the corresponding spectral response of our cascaded spherical cavities, show good agreement with theoretical and numerical calculations based on the multi-sphere Mie theory.³⁸ Unlike coupled disk resonators where modes can only propagate along the disk's plane, in our experiments, we observe high-Q resonances with an electromagnetic field showing significant energy density in the regions of the resonators removed from their equatorial planes [an equatorial plane is defined as the plane in which a fundamental whispering gallery modes (WGM) have been excited in a single resonator]. Such distributions of the electromagnetic field would originate from a combination of so-called high-order polar whispering gallery modes (modes whose plane of propagation is significantly inclined with respect to the equator). Our resonators also permit coupling between modes that propagate in different planes and exhibit many level-crossing events.

Spherical resonators can be formed by different types of interfaces of materials with different refractive indices: a solid-gas, a solid-liquid, 35 a liquid-gas, 38-40 or a liquid-liquid 13 interface. In this work, we use oil droplets in water, which form an almost perfectly spherical and smooth liquid-liquid interface, which we exploit to confine light and actuate these droplets as micro-resonators. This approach exploits the tendency of oil droplets, submerged in water, to acquire a spherical shape. Furthermore, a high degree of smoothness for spherical liquid-resonators significantly reduces scattering losses, which improves the quality factors 13,38-40 of the resonators. In addition, such droplets can be easily fabricated and manipulated with optical tweezers,³⁴ making them attractive for studying ensembles of high-Q resonators. Our method is scalable to as many droplets as needed. In fact, we can arrange any number of spheres in various structures such as a linear chain, a circular array, or any other structure, including 3D.

II. EXPERIMENTAL SETUP

In our experiment (Fig. 1), we submerge oil droplets (Sigma-Aldrich, Immersion oil, 56822-50ML, n = 1.516) in water and use them as resonators (Methods). The realization of our optical tweezers setup was inspired by the publication of Fällman.⁴¹ Droplets of $75 \pm 1 \mu m$ diameter are dragged, using optical tweezers,³⁴ to form various configurations of cascaded resonators near a tapered-fiber

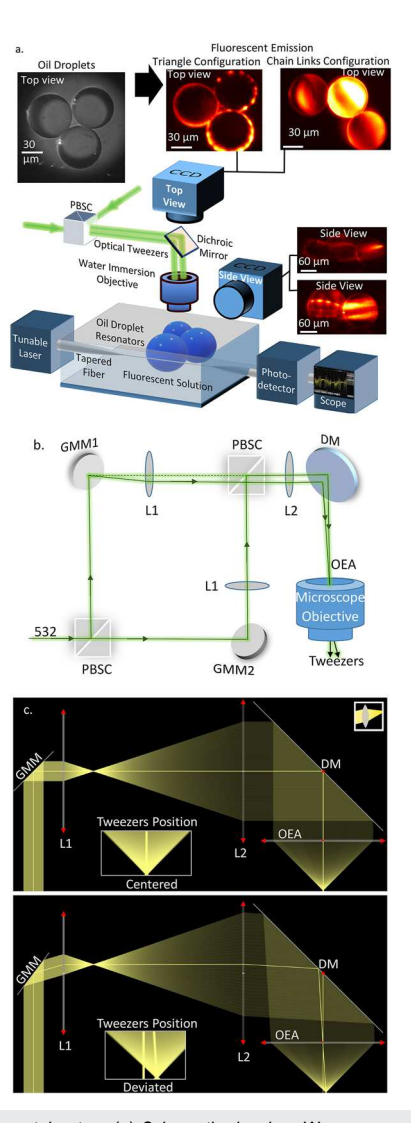


FIG. 1. Experimental setup. (a) Schematic drawing. We arrange oil droplet resonators next to a tapered-fiber coupler by using optical tweezers. A tunable laser is coupled to the spheres' ensemble via one side of the fiber, while the spectral transmission is measured using a photodiode at the other side of the fiber. At the same time, we film the modes by doping the water with a fluorescent material, using a side-view camera and a top-view camera to capture the spatial distribution of the mode while the frequency of a tunable laser sweeps through the ensemble's resonances. Both tapered fiber and resonators are submerged in water. The objective is wet (Nikon CFI, Apochromat NIR 60×, W), its numerical aperture is 1.0, and its working distance is 2.8 mm. (b) A detailed drawing of our double-tweezer system, where a gimbal mount mirror (GMM1) is used to control the position of the first tweezers, and a GMM2 is used to control the positions of the second tweezers. We use polarizing beam splitter cubes (PBSC) to split and combine the tweezers beams. Overfilling the objective entrance aperture (OEA) with the entering beam is achieved by imaging the gimbal mount mirror surface onto OEA using a 4-F system where lenses are labeled with L1 and L2. All those factors make it possible to manipulate submerged 100 μ m diameter oil resonators with 0.4 W, 532 nm (0.2 W per tweezers) input power. We use a dichroic mirror (DM) to prevent the top-view image acquisition camera from accepting the tweezers' light. The DM and PBSCs also make the power efficiency of our two-tweezers system to be almost 100%. (c) Schematic of tweezers position at the plane of interest. Beam position deviation (2D), as a result of a change in spatial orientation of GMM, (open-source web application: Ray Optics Simulation).

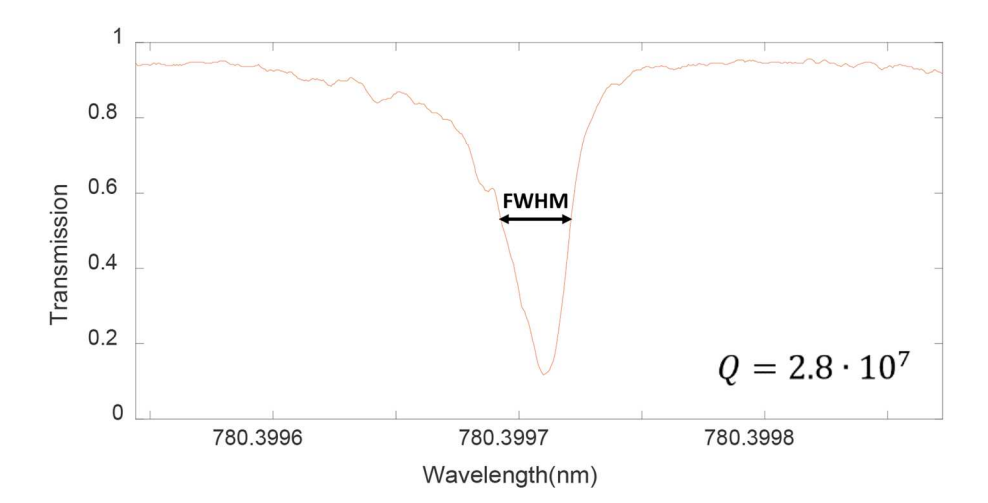


FIG. 2. Resonator quality factor. The resonator linewidth prior to adding fluorescent dye into cladding reveals a quality factor of 28×10^6 . Droplet diameter is 75 \pm 1 μm and operation is at the undercoupled regime where transmission drops to 15%

coupler 13,34 that brings light from a tunable laser, at 765-781 nm, into the cascaded resonators. Input power was 1 mW, and droplets were tested individually, using a microscope to have an equal diameter to within our microscope resolution, which was 1 μ m. The spectral transmission of the sphere cluster is monitored while scanning the laser wavelength through resonances by connecting the output side of the tapered fiber to a photodiode. Coupling is at the under-coupled regime, where transmission drops to 15%. A typical experiment, such as in Fig. 4, takes about 10 min, during which the resonators' ensemble did not change its optical properties. We did not notice a spontaneous motion of the droplets. After examining one droplet configuration, we reused them by arranging them in a different configuration. We could couple light to a resonator's ensemble 24 h after its fabrication, but we did not explicitly study the aging of a specific droplet configuration. In the past, we could solidify liquid droplets in polymer environments to last for years.⁴² We believe similar solidification is also possible for coupled-resonator like the ones we report here.

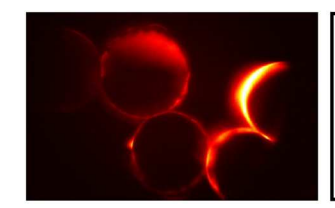
In detail, while scanning the optical wavelength, we film various resonances using the fluorescent mode mapping technique, 35 where the fluorescent material dissolved in water converts the resonating light into emission at a different color so that we can use a filter to selectively photograph fluorescence. This fluorescent emission originates from places near the oil-water interface where both resonating light and fluorescent material exist. The fluorescent emission is incoherent and non-directional and is, therefore, expected to benefit higher-resolution images and more light reaching the camera. Indeed, according to our experience, images relying on fluorescence are better when compared to images relying on resonant light, which is coherent and reaches the camera in small quantities and only from places where scatterers exist. The configuration of the spherical resonator ensemble permits light propagation in various planes and, hence, stands in contrast with planar configurations such as coupled rings, where only one top-view camera is required to image the planer modes. For this reason, we use a set of two microscopes for imaging the fluorescent emission, one from the side and the other from the top (Fig. 1). Since the fluorescent medium surrounds the droplet, it is affected only by evanescent light⁴³ extending from the droplets into water cladding. The fact that we image only

light that originated from a thin layer near the oil—water interface improves the certainty of knowing where the light originates from and benefits the quality of the images, given that the microscope's depth of focus is limited.

Regarding the influence of the fluorescent material on the optical quality—by adding a fluorescent dopant—one trades off reduction in the optical quality factor, Q, for the ability to map the spatial structure of the modes. In our work, we find that fluorescently imaging the modes improves with fluorescent concentration such that Q falls to $\sim 10^6$. The typical optical quality factor, Q, for our resonators is $Q=10^7$ for experiments with no fluorescent marker (see methods, Fig. 2).

III. EXPERIMENTAL RESULTS

We start with a five-sphere ensemble, which we call a quintet, and fluorescently photograph one of its modes (Fig. 3). This mode is exited using a 770 nm laser and a tapered fiber near the left-hand side sphere, as depicted in Fig. 3. One can see in Fig. 3 that one of the spheres exhibits stronger fluorescent radiation and that another sphere exhibits interference fringes that are spread along its circumference. We find that these behaviors are typical to our multi-sphere ensembles and will discuss these mode shapes in more detail in what follows.



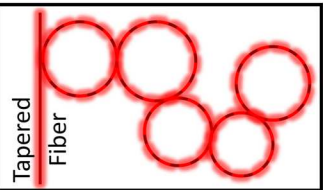


FIG. 3. Five spheres experiment (quintet). Fluorescent mapping for one of the resonances. A tapered fiber coupler (not visible) is near the left sphere. In this figure, the only constraint on the number of spheres relates to our microscope's limited field of view.

We now arrange three droplets of equal size into a chain shape, which we call a "chained trio." Subsequently, we optically interrogate the chain trio, via one of the resonators, while slowly scanning the input light at the 765–770 nm spectral band (Fig. 4). We monitor the spectral transmission of the chained trio while scanning the optical wavelength through the resonances (Fig. 4, top). At the same time, modes are fluorescently filmed to reveal their structure [Figs. 4(a)-4(f)]. As expected, each spectral absorption line is

accompanied by a flash of fluorescent light at a spatial shape we record. Together, the transmission spectrum and photographs provide a spatial-spectral signature of the ensemble's resonances. One can see that line widths in Fig. 4 are thermally broadened.²⁸

The violation of spherical symmetry of individual resonators in our coupled structures results in lifting of the degeneracy between modes with the same orbital number l, but different polar numbers m (m distinguishes between modes with different inclinations with

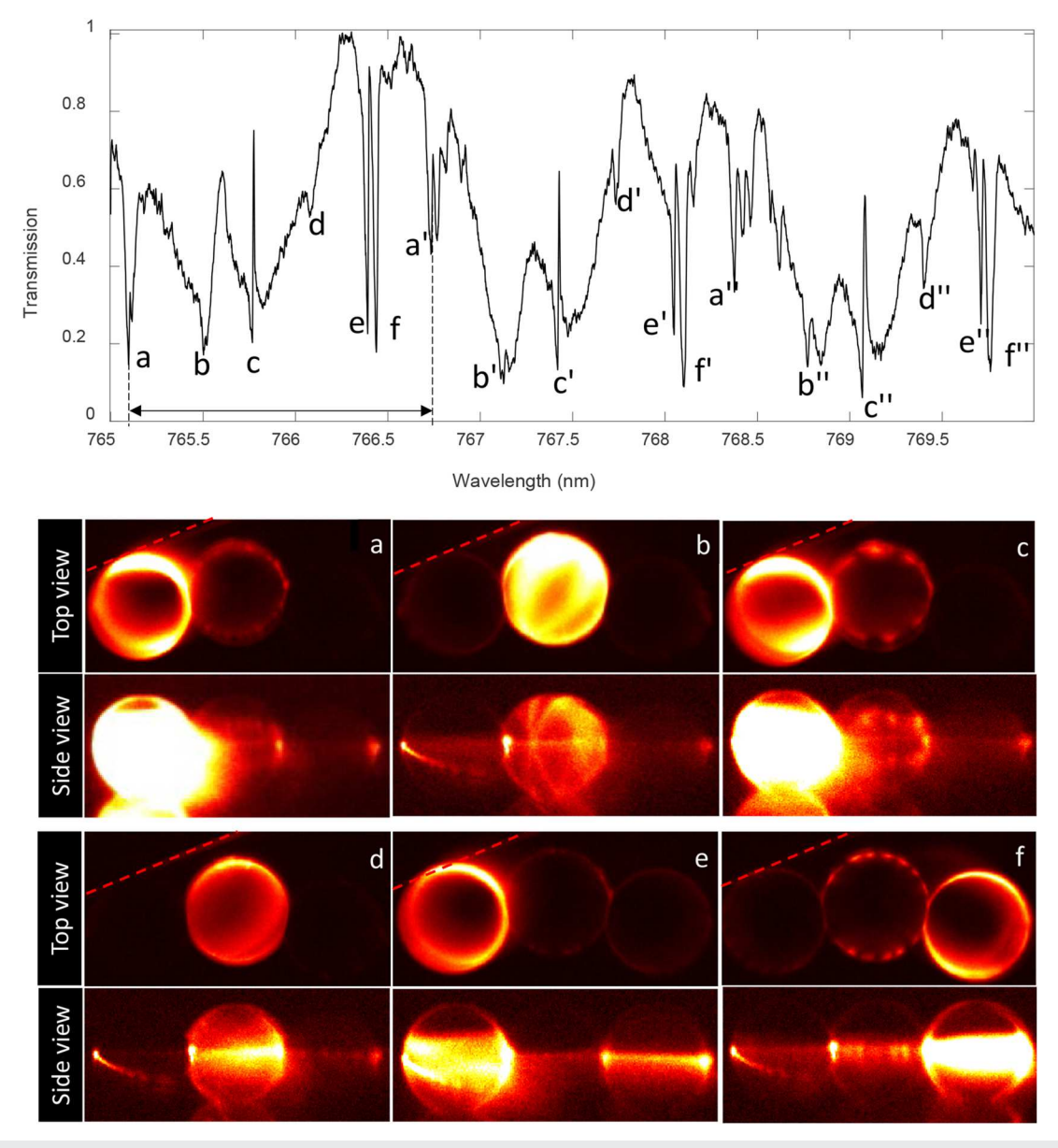


FIG. 4. Chain-configuration experiment. (Above) The transmission spectrum of the chain where resonances are marked with (a)–(f), their repetition after one free spectral range is marked with (a")–(f"). The free spectral range is marked using a double-headed arrow. (Below) Fluorescent mapping of the chain's modes. Photographs (a)–(f) correspond to resonances (a)–(f) that as marked on the graph. The tapered fiber is marked with a dashed line. The taper is coupled to only the left-hand side resonator (see Visualization 1 and Visualization 2 supplementary material).

respect to the equator in individual resonators and remains a good characteristic of the collective modes of the chain in linear chains provided that it is defined with respect to the polar axes chosen along the chain). This results in the appearance of a large number of spectrally and spatially overlapping modes. This overlap between the modes manifests as interference patterns seen along the drop's circumference [e.g., Fig. 4(f)].

Figure 4 shows a seven-mode group that repeats itself after one free spectral range and two free spectral ranges. We denote the first appearance of this seven-mode group using the letters (a)–(g) (Fig. 4, top), their second appearance using (a')–(g'), and their third one

as (a")–(g"). Mode a is separated by 1.7 nm from (a') (horizontal double-headed arrow, Fig. 4, top) and 2 × 1.7 nm² from mode (a"). This type of separation repeats itself for resonances (b)–(g). Interestingly, this 1.7 nm separation corresponds to the free spectral range of a single sphere. The droplet diameter corresponding to this measured 1.7 nm free spectral range is 73 μ m, which slightly deviates from 75 μ m measured with a microscope. Importantly, modes (a)–(f) are not only a family in the spectral domain but also in the spatial domain, meaning that mode "(a)" looks like modes (a') and (a") and so on. As for the spatial structure of each mode, in most of the chained trio's resonances, one sphere is photographed to be

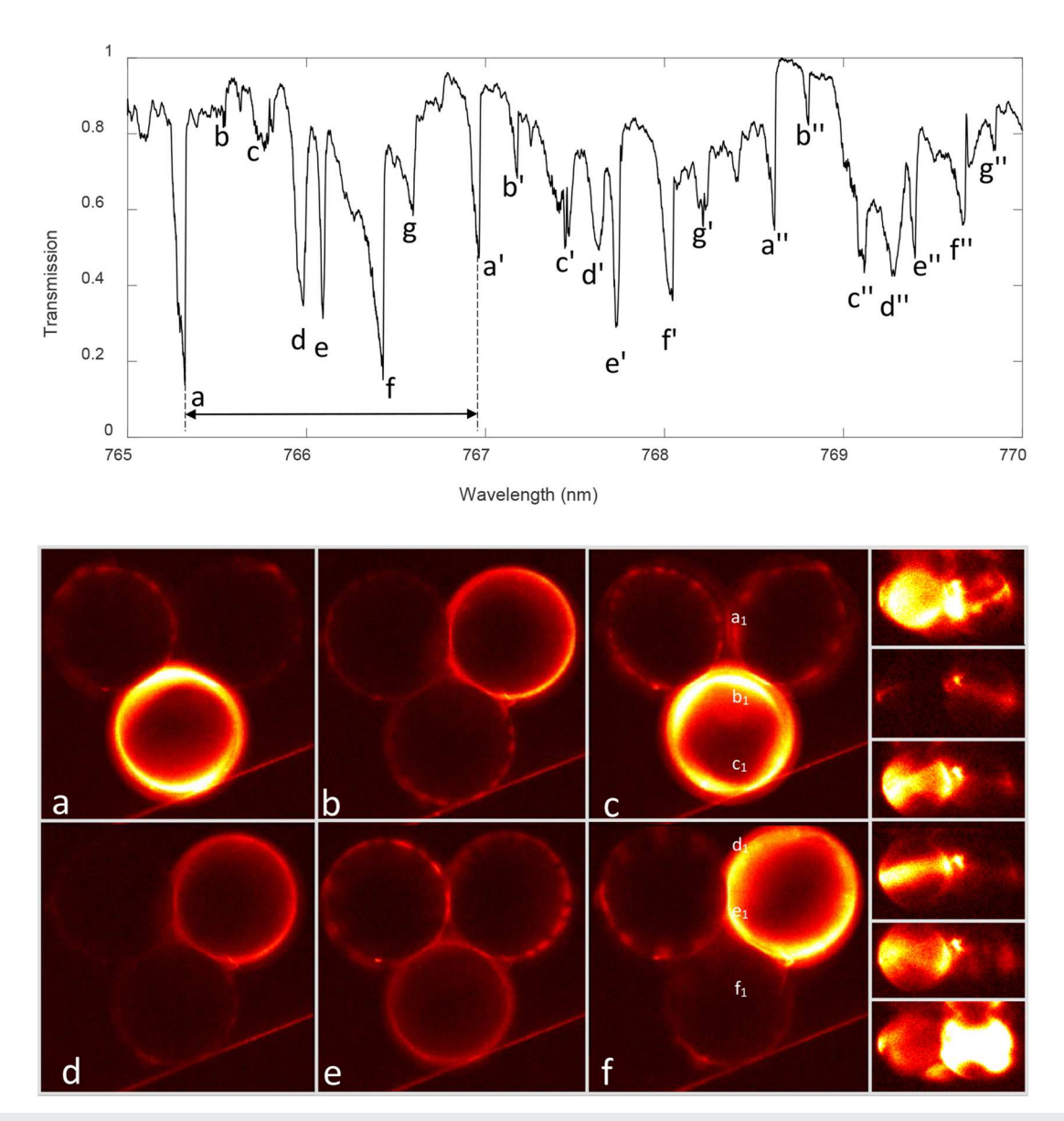


FIG. 5. Triangular configuration experiment. Transmission spectrum and related fluorescent mode mapping. Formalism here is similar to the one in Fig. 4. (a)–(f) Top view, (a1)–(f1) side view. (See Visualization 3 and Visualization 4 supplementary material).

fluorescently brighter than the others [e.g., Fig. 4(b)], meaning that this sphere either carries a higher intensity or that its mode is further evanescently extending to the surrounding.

The repeating feature of the spectrum of a linear chain of spheres was first observed in numerical simulations of Ref. 44 under the assumption of perfectly aligned resonators. The authors of that work found that the spectrum of a chain of spheres with an odd number of elements (3 in our case) always contains a frequency of a single sphere resonance, which is surrounded by resonances resulting from lifting the degeneracy of the whispering gallery modes with respect to the polar number m as explained above (satellite resonances). This lifted degeneracy explains the repeating pattern of the resonance groups, coinciding with the distribution of single sphere resonances, similar to what we experimentally observed (Fig. 4). While the exact positions, shapes, and strengths of the satellite resonances depend on the inter-mode coupling, the Q-factor, and the frequency of the single sphere resonances, these parameters do not change much for spectrally close single-sphere resonances, explaining why satellite resonances form around single-sphere peaks also look similar.

A simple analytical analysis of a three-sphere situation in Ref. 44 shows that for the mode corresponding to the single resonance frequency, one should expect an almost zero field intensity in the middle sphere accompanied by identical fields in two terminal-spheres. For other modes, the middle sphere is expected to have maximum intensity while the intensities of the first and the third spheres are diminished. The latter distribution of intensities is seen in Figs. 4(b) and 4(d), while the former is also manifested (Fig. 7, top). We do see a distribution of intensities in which the second

sphere goes "dark," but the symmetry between the first and the third sphere does not manifest itself. Such a behavior is explained by the deviations of a three-sphere configuration from the strictly one-dimensional arrangement. We have extended numerical simulations of Ref. 44 to allow for the center of the third sphere to be displaced from the line connecting the centers of the first and the second and observed intensity distributions similar to those seen in the experiment (details of the computations will be published elsewhere). Some resonances include a necklace-type shape [e.g., Fig. 4(f), central sphere]. This shape originates from the interference pattern between two modes with a different principal quantum number but with resonance frequencies positioned within resonance linewidth from each other. This phenomenon is generally referred to as level crossing since the resonance frequencies of two modes cross by changing a parameter. 35-37 It is also common to refer to this necklace-shaped mode as stopped light,³⁵ since its group velocity is zero. We found that level crossing is more abundant in cascaded resonators when compared to a single droplet spectrum. This level crossing abundance in coupled resonators is due to the lifting of the degeneracy between the modes with different polar numbers m.

Also, with the increasing number of resonators, more modes are available to overlap, making the spectrum of the resonances almost continuous. To understand this phenomenon, one just needs to notice that with an increasing number of resonators, the spectral interval between modes with orbital numbers l and l + 1 must be filled with N(2l + 1) (N here is the number of resonators) distinct modes, which have finite spectral widths and, therefore, strongly overlap resulting in the observed interference patterns and

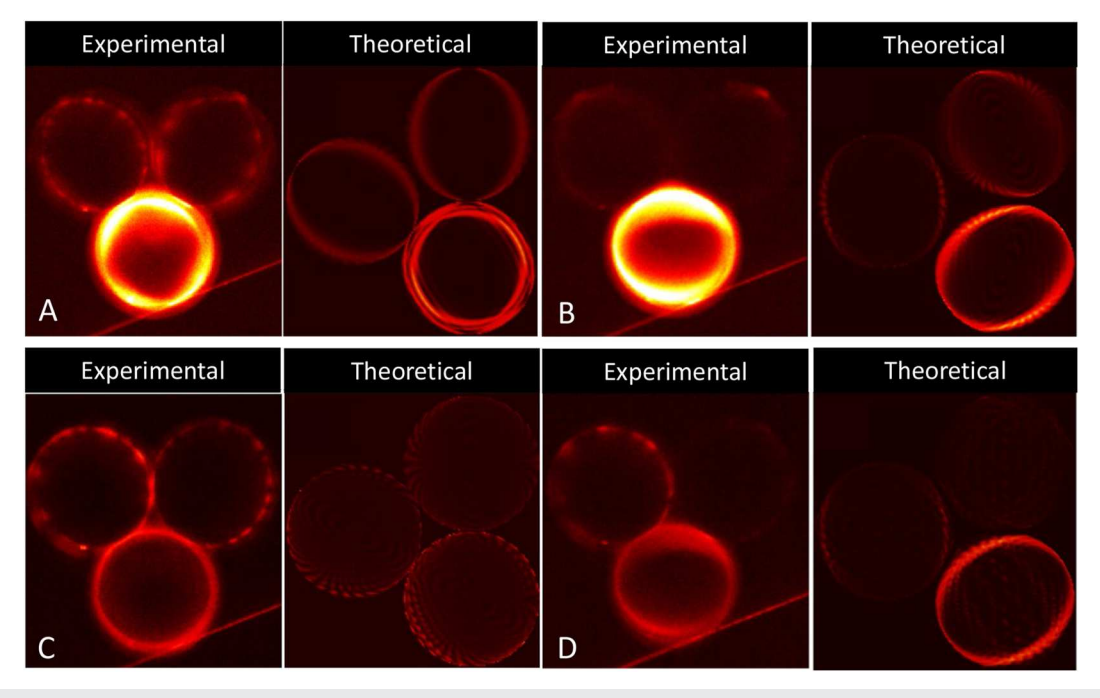


FIG. 6. Experimental results and their corresponding simulation for a triangular shape. Note the 0 shaped resonances [(b) and (d)], the flower shapes originating from level crossing (c), and the fact one sphere is sometimes brighter than the others [(a) and (b)] (see Visualization 5 and Visualization 6 supplementary material).

quasi-continuum of resonances. From a practical view, this ability to resonantly respond to white light⁴⁵ can be used in the future for white light sources that are as bright as lasers. Such technological ability to provide white light from a single-mode fiber is challenging, particularly in the case of a continuous wave (CW) source. We also experimentally studied spectra and spatial distribution of the intensity for a system of three resonators arranged in an equilateral triangle shape. Furthermore, we carried out numerical simulation of this configuration (Fig. 6) and compared the results of the simulations with the experimental results (Fig. 5).

The triangular arrangement of the resonators differs from the linear chain by its symmetry: while the linear chain preserves an axial rotational symmetry around the line connecting the centers of the resonators so that all modes of the chain can be characterized by a "polar" quantum number m, the triangular arrangement has only discrete symmetry of an equilateral triangle, so that the modes of this configuration are combinations of whispering gallery modes (WGM) with different "polar" numbers. The total number of modes is the same as in the linear case, but since the spectral widths and mutual positions of the resonances are different, the number of observed resonance peaks is also different. The actual experimental configuration of the resonators deviates from the ideal symmetrical form, but certain experimentally observed intensity distributions are pretty close to those generated in the computer simulations [e.g., Figs. 6(a) and 6(c)]. The overlap between different modes is as significant in this case as in the linear one, so the formation of interference patterns resulting from simultaneous excitation of

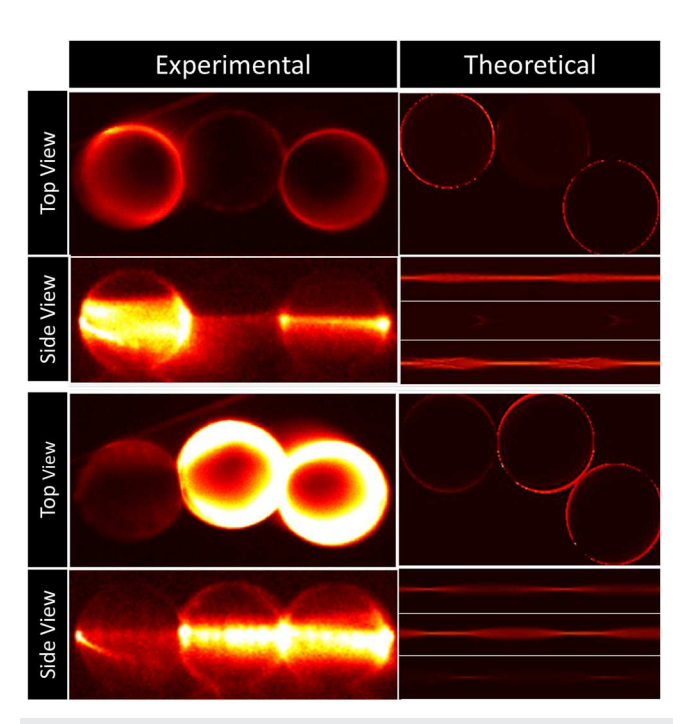


FIG. 7. Experimental results and their corresponding simulation for a chain shape. Note the fact one sphere is sometimes darker than the others [(a) and (b)]. The side view theoretical results presented here as flattened sphere surfaces, with vertical axis: 0 to π and horizontal axis: 0 to 2π . (see Visualization 7 and Visualization 8 supplementary material).

different modes with almost the same frequencies (level crossing) is as abundant.

Our simulations of both linear and triangular photonic molecules (Figs. 6 and 7) were conducted using generalized multisphere Mie theory in the so-called resonant approximation. This approximation neglects to couple between single sphere resonances characterized by different orbital numbers l and different polarizations. This approximation might miss the occasional quasi degeneracy of the resonances with different orbital numbers, but it captures the main features of the spectra of the multi-sphere configurations, as can be seen from the comparison of our calculations with experimental results.

In conclusion, we cascade spherical resonators to construct ensembles of cavities. The resonator ensembles have families of modes, with each family member repeating itself every free spectral range while maintaining its spatial and spectral shape. Despite their relatively large mode volume, such arrays can combine gain³⁸ and an almost continuous spectrum (Fig. 4) that might impact spectrally continuous emitters for applications where white light is needed to come from a single-mode fiber. Our work is scalable to large ensembles made of many high Q cavities, that one can solidify⁴² upon need.

SUPPLEMENTARY MATERIAL

See the supplementary material for a system stability check, using one droplet resonator and completing the full range scan of 765–781 nm, that we first perform. If there is no drift over the scan time, we start the experiment by measuring the Q-factor of one droplet to represent the hole batch. Droplets used in cascaded configurations were chosen against known reference to have similar diameters of $75 \pm 1~\mu m$. Droplets were tested individually, using a microscope, to have an equal diameter within our microscope resolution of $1~\mu m$. The laser input power used during the scan is 1~mW. Coupling to well-coffined modes can be considered critical. The fluorescent dye used in our experiment is ADS780WS, which has absorption and emission peaks at 780 and 813 nm, respectively. Our longest experiment took 2~h during which the droplets did not move and the spectrum was repeatable. In the past, we were solidifying liquid droplets in polymer environments to last for years. 42

Submerged oil droplet material: Sigma-Aldrich, Immersion oil, 56822-50ML, n=1.516.

Fluorescent dye: Adsdyes—American Dye Source, ADS780WS.

ACKNOWLEDGMENTS

This research was supported by the United States–Israel Binational Science Foundation (BSF) (Grant Nos. 2016670 and 2020683), the U.S. National Science Foundation (NSF) (Grant Nos. 1711801 and ECCS1711451), ICore: the Israeli Excellence Center "Circle of Light," Grant No. 1802/12, and the Israeli Science Foundation, Grant Nos. 537/20 and 1572/15.

AUTHOR DECLARATIONS

Conflict of Interest

The authors have no conflicts to disclose.

Author Contributions

Stanislav Kreps: Investigation (equal); Writing – original draft (equal). Vladimir Shuvayev: Data curation (equal). Mark Douvidzon: Methodology (equal). Baheej Bathish: Data curation (equal). Tom Lenkiewicz Abudi: Investigation (equal). Amirreza Ghaznavi: Conceptualization (equal). Jie Xu: Formal analysis (equal). Yang Lin: Conceptualization (equal). Lev Deych: Supervision (equal). Tal Carmon: Supervision (equal).

DATA AVAILABILITY

The data that support the findings of this study are available from the corresponding author upon reasonable request.

REFERENCES

- ¹ K. J. Vahala, "Optical microcavities," Nature 424, 839–846 (2003).
- ²D. V. Strekalov, C. Marquardt, A. B. Matsko, H. G. L. Schwefel, and G. Leuchs, "Nonlinear and quantum optics with whispering gallery resonators," J. Opt. 18, 123002 (2016).
- ³Y.-n. Zhang, T. Zhou, B. Han, A. Zhang, and Y. Zhao, "Optical bio-chemical sensors based on whispering gallery mode resonators," Nanoscale **10**, 13832–13856 (2018).
- ⁴J. Li, M.-G. Suh, and K. Vahala, "Microresonator Brillouin gyroscope," Optica 4, 346 (2017).
- ⁵P. Del'Haye *et al.*, "Optical frequency comb generation from a monolithic microresonator," Nature **450**, 1214–1217 (2007).
- ⁶B. Min *et al.*, "Erbium-implanted high-Q silica toroidal microcavity laser on a silicon chip," Phys. Rev. A **70**, 033803 (2004).
- ⁷S. M. Spillane, T. J. Kippenberg, and K. J. Vahala, "Ultralow-threshold Raman laser using a spherical dielectric microcavity," Nature **415**, 621–623 (2002).
- ⁸T. Carmon and K. J. Vahala, "Visible continuous emission from a silica microphotonic device by third-harmonic generation," Nat. Phys. 3, 430–435 (2007).
- ⁹C. H. Metzger and K. Karrai, "Cavity cooling of a microlever," Nature 432, 1002–1005 (2004).
- ¹⁰T. Carmon, H. Rokhsari, L. Yang, T. J. Kippenberg, and K. J. Vahala, "Temporal behavior of radiation-pressure-induced vibrations of an optical microcavity phonon mode," Phys. Rev. Lett. 94, 223902 (2005).
- phonon mode," Phys. Rev. Lett. **94**, 223902 (2005). ¹¹I. S. Grudinin, A. B. Matsko, and L. Maleki, "Brillouin lasing with a CaF₂ whispering gallery mode resonator," Phys. Rev. Lett. **102**, 043902 (2009).
- ¹²M. Tomes and T. Carmon, "Photonic micro-electromechanical systems vibrating at *X*-band (11-GHz) rates," Phys. Rev. Lett. **102**, 113601 (2009).
- ¹³S. Kaminski, L. L. Martin, S. Maayani, and T. Carmon, "Ripplon laser through stimulated emission mediated by water waves," Nat. Photonics 10, 758–761 (2016)
- ¹⁴S. T. Chu, B. E. Little, W. Pan, T. Kaneko, and Y. Kokubun, "Cascaded microring resonators for crosstalk reduction and spectrum cleanup in add-drop filters," IEEE Photonics Technol. Lett. **11**, 1423 (1999).
- ¹⁵ A. Yariv, Y. Xu, R. K. Lee, and A. Scherer, "Coupled-resonator optical waveguide: A proposal and analysis," Opt. Lett. 24(11), 711–713 (1999).
- ¹⁶V. N. Astratov, J. P. Franchak, and S. P. Ashili, "Optical coupling and transport phenomena in chains of spherical dielectric microresonators with size disorder," Appl. Phys. Lett. 85, 5508–5510 (2004).
- ¹⁷D. U. Smith, H. Chang, K. A. Fuller, A. T. Rosenberger, and R. W. Boyd, "Coupled-resonator-induced transparency," Phys. Rev. A 69, 063804 (2004).
- ¹⁸Z. Chen, A. Taflove, and V. Backman, "Highly efficient optical coupling and transport phenomena in chains of dielectric microspheres," Opt. Lett. **31**(3), 389–391 (2006).
- ¹⁹M. J. Hartmann, F. G. S. L. Brandão, and M. B. Plenio, "Strongly interacting polaritons in coupled arrays of cavities," Nat. Phys. 2(12), 849–855 (2006).

- ²⁰ M. Notomi, E. Kuramochi, and T. Tanabe, "Large-scale arrays of ultrahigh-Q coupled nanocavities," Nat. Photonics 2(12), 741–747 (2008).
- ²¹E. Gil-Santos *et al.*, "Light-mediated cascaded locking of multiple nano-optomechanical oscillators," Phys. Rev. Lett. **118**, 063605 (2017).
- ²²Y. Yin, Y. Niu, L. Dai, and M. Ding, "Cascaded microbottle resonator and its application in add-drop filter," IEEE Photonics J. 10, 7103810 (2018).
- ²³B. Peng *et al.*, "Parity-time-symmetric whispering-gallery microcavities," Nat. Phys. **10**, 394 (2014).
- ²⁴H. Wang *et al.*, "Polarization-independent tunable optical filter with variable bandwidth based on silicon-on-insulator waveguides," Nanophotonics 7, 1469–1477 (2018).
- ²⁵ A. A. Savchenkov, V. S. Ilchenko, A. B. Matsko, and L. Maleki, "High-order tunable filters based on a chain of coupled crystalline whispering gallery-mode resonators," IEEE Photonics Technol. Lett. 17, 136–138 (2005).
- ²⁶Y. Hu *et al.*, "High-speed silicon modulator based on cascaded microring resonators," Opt. Express **20**, 15079 (2012).
- ²⁷H.-T. Kim and M. Yu, "Cascaded ring resonator-based temperature sensor with simultaneously enhanced sensitivity and range," Opt. Express 24, 9501 (2016).
- ²⁸T. Carmon, L. Yang, and K. J. Vahala, "Dynamical thermal behavior and thermal self-stability of microcavities," Opt. Express 12, 4742–4750 (2004).
- ²⁹Y. Hara, T. Mukaiyama, K. Takeda, and M. Kuwata-Gonokami, "Heavy photon states in photonic chains of resonantly coupled cavities with supermonodispersive microspheres.," Phys. Rev. Lett. 94, 203905 (2005).
- ³⁰B. M. Möller, U. Woggon, M. V. Artemyev, and R. Wannemacher, "Photonic molecules doped with semiconductor nanocrystals," Phys. Rev. B **70**, 115323 (2004).
- ³¹B. Li, C. P. Ho, and C. Lee, "Tunable Autler-Townes splitting observation in coupled whispering gallery mode resonators," IEEE Photonics J. **8**, 4501910 (2016)
- ³² A. Chiasera *et al.*, "Spherical whispering-gallery-mode microresonators," Laser Photonics Rev. 4, 457–482 (2010).
- ³³T. Carmon, M. C. Cross, and K. J. Vahala, "Chaotic quivering of micron-scaled on-chip resonators excited by centrifugal optical pressure," Phys. Rev. Lett. 98, 167203 (2007).
- 34S. Kaminski, L. L. Martin, and T. Carmon, "Tweezers controlled resonator," Opt. Express 23, 28914 (2015).
- ³⁵A. A. Savchenkov, A. B. Matsko, V. S. Ilchenko, D. Strekalov, and L. Maleki, "Direct observation of stopped light in a whispering-gallery-mode microresonator," Phys. Rev. A 76, 023816 (2007).
- ³⁶T. Carmon *et al.*, "Static envelope patterns in composite resonances generated by level crossing in optical toroidal microcavities," Phys. Rev. Lett. **100**, 103905 (2008).
- ³⁷S. T. Attar, V. Shuvayev, L. Deych, L. L. Martin, and T. Carmon, "Level-crossing and modal structure in microdroplet resonators," Opt. Express **24**, 13134 (2016).
- ³⁸S. Maayani and T. Carmon, "Droplet Raman laser coupled to a standard fiber," Photonics Res. 7, 1188 (2019).
- ³⁹S. Maayani, L. L. Martin, and T. Carmon, "Water-walled microfluidics for high-optical finesse cavities," Nat. Commun. 7, 10435 (2016).
- ⁴⁰J. Kher-Alden *et al.*, "Microspheres with atomic-scale tolerances generate hyperdegeneracy," Phys. Rev. X 10, 031049 (2020).
- ⁴¹E. Fällman and O. Axner, "Design for fully steerable dual-trap optical tweezers," Appl. Opt. **36**, 2107 (1997).
- ⁴²M. Davidson *et al.*, "Toward transformable photonics: Reversible deforming soft cavities, controlling their resonance split and directional emission," APL Photonics **6**, 071304 (2021).
- ⁴³M. Tomes, K. J. Vahala, and T. Carmon, "Direct imaging of tunneling from a potential well," Opt. Express 17, 19160 (2009).
- ⁴⁴L. I. Deych, C. Schmidt, A. Chipouline, T. Pertsch, and A. Tünnermann, "Propagation of the fundamental whispering gallery modes in a linear chain of microspheres," Appl. Phys. B: Lasers Opt. **93**, 21–30 (2008).
- ⁴⁵A. A. Savchenkov, A. B. Matsko, and L. Maleki, "White-light whispering gallery mode resonators," Opt. Lett. **31**, 92 (2006).